UCSF
UC San Francisco Previously Published Works

Title

Acetylcholine Receptor (AChR) Clustering Is Regulated Both by Glycogen Synthase Kinase 3β (GSK3β)-dependent Phosphorylation and the Level of CLIP-associated Protein 2 (CLASP2) Mediating the Capture of Microtubule Plus-ends*

Permalink

https://escholarship.org/uc/item/9bf6n4kf

Journal

Journal of Biological Chemistry, 289(44)

ISSN

0021-9258

Authors

Basu, Sreya
Sladecek, Stefan
Pemble, Hayley
et al.

Publication Date

2014-10-01

DOI

10.1074/jbc.m114.589457

Peer reviewed

eScholarship.org Powered by the California Digital Library
University of California

THE JOURNAL OF BIOLOGICAL CHEMISTRY VOL. 289, NO. 44, pp. 30857–30867, October 31, 2014
© 2014 by The American Society for Biochemistry and Molecular Biology, Inc. Published in the U.S.A.

Acetylcholine Receptor (AChR) Clustering Is Regulated Both by Glycogen Synthase Kinase 3β (GSK3β)-dependent Phosphorylation and the Level of CLIP-associated Protein 2 (CLASP2) Mediating the Capture of Microtubule Plus-ends*

Received for publication, June 13, 2014, and in revised form, September 13, 2014 Published, JBC Papers in Press, September 17, 2014, DOI 10.1074/jbc.M114.589457

Sreya Basu[‡§1], Stefan Sladecek[‡1], Hayley Pemble[¶], Torsten Wittmann[¶], Johan A. Slotman[‖], Wiggert van Cappellen[‖], Hans-Rudolf Brenner[‡2], and Niels Galjart[§3]

From the [‡]Institute of Physiology, Department of Biomedicine, University of Basel, CH-4056 Basel, Switzerland, the [§]Department of Cell Biology, Erasmus Medical Center, 3015 GE, Rotterdam, Netherlands, the [¶]Department of Cell and Tissue Biology, University of California at San Francisco, San Francisco, California 94143, and [‖]Optical Imaging Center, Erasmus Medical Center, 3015 GE Rotterdam, Netherlands

Background: The plus-end-binding protein CLASP2 was shown to regulate MT capture at the neuromuscular junction.
Results: GSK3β-mediated CLASP2 phosphorylation regulates CLASP2-MT binding and AChR insertion at synaptic clusters.
Conclusion: The agrin-induced control of CLASP2 phosphorylation is an important mechanism for MT capture and synaptic AChR clustering.
Significance: Agrin-induced AChR delivery to synaptic AChR clusters through CLASP2-mediated MT capture ensures efficient clustering of AChRs at the synaptic muscle membrane.

The postsynaptic apparatus of the neuromuscular junction (NMJ) traps and anchors acetylcholine receptors (AChRs) at high density at the synapse. We have previously shown that microtubule (MT) capture by CLASP2, a MT plus-end-tracking protein (+TIP), increases the size and receptor density of AChR clusters at the NMJ through the delivery of AChRs and that this is regulated by a pathway involving neuronal agrin and several postsynaptic kinases, including GSK3. Phosphorylation by GSK3 has been shown to cause CLASP2 dissociation from MT ends, and nine potential phosphorylation sites for GSK3 have been mapped on CLASP2. How CLASP2 phosphorylation regulates MT capture at the NMJ and how this controls the size of AChR clusters are not yet understood. To examine this, we used myotubes cultured on agrin patches that induce AChR clustering in a two-dimensional manner. We show that expression of a CLASP2 mutant, in which the nine GSK3 target serines are mutated to alanine (CLASP2–9XS/9XA) and are resistant to GSK3β-dependent phosphorylation, promotes MT capture at clusters and increases AChR cluster size, compared with myotubes that express similar levels of wild type CLASP2 or that are noninfected. Conversely, myotubes expressing a phosphomimetic form of CLASP2 (CLASP2– 8XS/D) show enrichment of immobile mutant CLASP2 in clusters, but MT capture and AChR cluster size are reduced. Taken together, our data suggest that both GSK3β-dependent phosphorylation and the level of CLASP2 play a role in the maintenance of AChR cluster size through the regulated capture and release of MT plus-ends.

The major presynaptic organizer of postsynaptic differentiation at the neuromuscular junction (NMJ)[4] is agrin (1–3), a heparan sulfate proteoglycan secreted from the motor nerve terminal and acting through its receptor/effector LRP4/MuSK in the muscle fiber membrane (4, 5). Agrin on its own is sufficient to induce differentiation of functional synaptic membranes *in vivo* in the absence of motor nerves, including a postsynaptic apparatus (6–8) that traps and anchors the acetylcholine receptors (AChRs) at high density at the synapse (9–12). Another factor contributing to synaptic AChR clustering is the focal delivery of AChRs to the clusters through focal capturing of microtubules (MTs), with MT capturing depending on the MT plus-end tracking protein (+TIP) CLASP2 (13). Because agrin inactivates GSK3β in muscle cells (13), and inactivation of GSK3β stimulates CLASP2-mediated MT capturing at the leading edge of migrating cells (14–16), agrin may direct MTs to the synaptic membrane by a process involving GSK3β and CLASP2. However, the mechanisms of this process are not understood.

CLASP2 interactions with MTs are complex and involve indirect binding to growing MT ends through the "core" TIPs EB1 and EB3 as well as direct MT binding (15, 17). MT binding is mediated by multiple weaker affinity interactions, including the central arginine- and serine-rich intrinsically disordered

* This work was supported by the Swiss National Science Foundation, The Swiss Foundation for Research on Muscle Diseases, the Netherlands Organization for Scientific Research CW Grant 70059011, and ZonMW Grant 91208002 (to N. G.).
[1] Both authors contributed equally to this work.
[2] To whom correspondence may be addressed: Institute of Physiology, Dept. of Biomedicine, Klingelbergstrasse 50, CH-4056 Basel, Switzerland. Tel.: 41-61-267-1638/83; E-mail: Hans-Rudolf.Brenner@unibas.ch.
[3] To whom correspondence may be addressed: Dept. of Cell Biology and Genetics, Erasmus MC, P. O. Box 2040, 3000 CA Rotterdam, The Netherlands. Tel.: 31-10-7043163; E-mail: n.galjart@erasmusmc.nl.

[4] The abbreviations used are: NMJ, neuromuscular junction; MT, microtubule; AChR, acetylcholine receptor; SIM, structured illumination microscopy; TIRFM, total internal reflection microscopy; PFA, paraformaldehyde; ROI, region of interest; CLSM, confocal laser scanning microscopy; α-BTX, α-bungarotoxin.

region (18), as well as TOG-like MT-binding domains (19). Both direct and indirect CLASP MT bindings are inhibited by phosphorylation of an array of GSK3β sites in the middle of the protein (16, 20). Furthermore, mutation of potential GSK3 target serine residues within this domain to nonphosphorylatable alanine residues (CLASP2–9XS/A) enhances CLASP2 binding to MT ends, whereas mutation to the phosphomimetic residue aspartic acid (CLASP2–8XS/D) strongly reduces MT plus-end binding (20). In interphase cells, the C terminus of CLASP2 interacts with CLIPs (14), with the trans-Golgi network protein GCC185 (21), and with the cell cortex proteins LL5β and ELKS (22). Interestingly, LL5β is present at the NMJ and is involved in AChR clustering (23); however, it is not known whether it mediates CLASP2-dependent MT capture at the NMJ.

Here, we overexpressed GFP-tagged wild type CLASP2, nonphosphorylatable CLASP2–9XS/A, or phosphomimetic CLASP2-8XS/D in cultured myotubes grown on agrin patches to examine the role of GSK3-dependent CLASP2 phosphorylation in the regulation of agrin-induced MT capturing and focal delivery of AChRs to the cluster. Delivery was inhibited by a constitutively active mutant of GSK3β, an effect that was rescued by forced expression of CLASP2–9XS/A. Both the CLASP2–8XS/D mutant and the CLASP2–9XS/A mutant accumulated in AChR clusters, albeit with different dynamic behavior. In addition, the CLASP2–8XS/D mutant reduced and the CLASP2–9XS/A mutant promoted, respectively, MT capturing and AChR cluster size at agrin-induced AChR clusters. Our experiments suggest that agrin, through inactivation of GSK3β, locally inhibits GSK3β-dependent phosphorylation of CLASP2 near the agrin patch; in turn, this promotes CLASP2 binding to MTs near the patch to mediate local MT capturing. MT plus-end density at the cluster correlates with acetylcholine receptor cluster size, and we suggest that both GSK3β-dependent phosphorylation and the level of CLASP2 play a role in the maintenance of cluster size.

EXPERIMENTAL PROCEDURES

Plasmids and Constructs—Adenoviral mRFP-GSK3β-S9A expression construct as well as adenoviral wild type and mutant GFP-CLASP2 expression constructs (all covering amino acids 340–1362 of the CLASP2 isoform with accession number XP_291057.5) are described elsewhere (20).

Generation and Usage of Adenoviral and Lentiviral Particles—To generate adenoviral particles for protein expression in myotubes, adenoviral vectors were linearized by PacI digest to expose the viral long terminal repeats (LTRs), precipitated, washed, resuspended, and transfected into adenovirus-producing 293Ad cells. The next day medium was exchanged and cells were allowed to accumulate adenoviral particles intracellularly for 10–14 days, until visible regions of cytopathic effect were observed. Cells were then scraped off and centrifuged, and the pellet was resuspended in PBS and subjected to four consecutive freeze/thaw cycles using MeOH at −80 °C and cell thawing at 37 °C to release adenoviral particles into solution. Cell debris was collected by centrifugation at 3000 rpm for 15 min at room temperature. The supernatant containing viral particles was used to again infect 293Ad cells, to amplify the viral stock to high titer. After 3–5 days, when visible regions of cytopathic effect were observed, cells were harvested and processed as described above. Finally, viral supernatants were aliquoted and stored at −80 °C. In some cases, we were provided with ready-made adenoviral particles, which were either used directly or amplified in 293Ad cells as described above.

Antibodies and Chemicals—Polyclonal rabbit anti-human EB3 has been described (13). Other antibodies were commercial products as follows: anti-GFP (chicken, Invitrogen) and anti-α-tubulin (rat, Abcam). Secondary antibodies were Alexa-conjugated goat anti-rabbit, goat anti-mouse, or goat anti-rat antibodies (Invitrogen) as well as donkey anti-chicken (Jackson ImmunoResearch). AChRs were labeled with α-BTX-Alexa488, -594, or -647 (Invitrogen) as indicated. Antibiotic/antimycotic solution was purchased from Invitrogen, and basic FGF was purchased from Invitrogen.

Preparation of Primary Muscle Cultures—Neonatal leg muscles from C57Bl6 mice were minced and dissociated with collagenase type IV and dispase type II, and cells were plated on a laminin substrate in DMEM containing 2 mM glutamine, 20% FCS, 5 ng/ml recombinant human basic FGF, and 1% antibiotic/antimycotic solution. After 2 days, cells were resuspended in PBS by brief trypsinization, treated with rat monoclonal anti-mouse α7-integrin antibody, and purified using (magnetic) Dynabeads coated with sheep anti-rat IgG and a Dynal-MPC-L magnetic particle concentrator (24, 25). Myotubes were cultured on laminin-coated dishes focally impregnated with patches of agrin as described (13). For the preparation of the dishes, COS-1 cells, transfected with a plasmid coding for full-length chicken neural agrin (26), were seeded at a density of $7–20 \times 10^3$ cells per 30-mm laminin-coated culture dish. After 48 h, cells were extracted for 1 h in 2% Triton X-100 in PBS, followed by intense washing (6–8 times for 1 h in PBS) and myoblast seeding (25). Subsequent differentiation was in DMEM, 5% horse serum, and 1% antibiotic/antimycotic solution. It should be noted that throughout this study, unless specified, agrin was applied attached to the culture substrate rather than in solution to mimic the *in vivo* situation.

For gene delivery *in vitro* using conventional transfection, myoblasts were transfected at confluency, immediately before switching to fusion medium using FuGENE6 (Roche Applied Science). For adenoviral and lentiviral transduction, cells were infected after formation of myotubes, and cells were imaged 48 h post-viral infection.

Immunofluorescence—To stain +TIPs and other proteins, myotube culture dishes were dropped into −80 °C methanol for 45 min, then transferred to a 1:1 mixture of methanol and 4% PFA at −20 °C for 30 min, followed by 10 min in 4% PFA at room temperature and 10 min in 100 mM glycine at room temperature. Cells were then permeabilized and blocked in PBS, 0.5% Triton X-100, 20% normal goat serum (NGS) (4 °C, 60 min). Primary and secondary antibodies were diluted in blocking solution and were applied at 4 °C overnight (primaries) or at room temperature for 45 min (secondaries).

Confocal Microscopy—Confocal microscopy was performed as described before. Briefly, myotubes were imaged with an SP5 confocal scanning laser microscope (DMI 4000B; Leica) at a resolution of 1024 × 1024 pixels using an HCX PL APO ×100 objective (NA 1.46) or an ACS APO ×63 objective (NA 1.30).

Image stacks were acquired with a step size of 300 nm. For comparison of different samples, the same laser settings and gains were applied.

Total Internal Reflection Microscopy (TIRFM)—The dynamics of GFP-CLASP2 proteins at agrin-induced clusters were examined in primary mouse myotubes by TIRFM. Myotubes derived from C57Bl/6 mice were stained with α-BTX-594 for 30 min and then washed with prewarmed DMEM for 1 h prior to imaging. For viral infections, myotubes were infected with the indicated viral supernatants 2 days prior to imaging. Cells were imaged at 37 °C and 5% CO_2 in Krebs-Ringer solution (140 mM NaCl, 5 mM KCl, 1 mM Mg^{2+}, 2 mM Ca^{2+}, 20 mM Hepes, 1 mM NaHPO4, and 5.5 mM glucose) at pH 7.4. Images were acquired on an inverted Nikon TI Eclipse microscope fitted with a ×100 apo-TIRF objective from Nikon (NA = 1.49), using an EM-CCD camera (Evolve, Photometrics), with the 491- and 561-nm laser lines (20 milliwatt) using a filter block from Chroma, and the Lambda10-3 shutter. Focus was maintained throughout imaging with the help of a perfect focus system. For analyzing the time course of CLASP2 dephosphorylation, 10 nM soluble chicken agrin (27) was added to GFP-CLASP2-infected cultured myotubes for the indicated time points followed by fixation in 2% PFA. Cells were then treated with α-BTX-594 (1 μg/ml for 15 min), washed in PBS, and imaged using TIRF microscopy.

Structured Illumination Microscopy (SIM)—Fixed samples were imaged using the ELYRA PS.1 structured illumination microscope (Carl Zeiss AG, Jena, Germany). Images were acquired using a ×63/1.40 oil plan apochromat objective and an Andor iXon DU 885 EMCCD camera. Stacks of images of cultured myotubes were acquired at a step size of 0.140 μm. Image processing was performed using the Zeiss Zen software. For co-localization experiments, precise pixel alignment between different acquisition channels was ensured by correcting potential pixel shifts via the channel alignment function within the Zen software (Zeiss). Maximum intensity projections were generated using Fiji (28).

+TIP Dynamics—For TIRF imaging of GFP-CLASP2-infected cells, images were acquired at one frame/s for 160–180s with an exposure time of 500 ms. Dynamics of CLASP2 comets inside and outside agrin-induced AChR clusters were analyzed using ImageJ. A maximum intensity projection of 180 frames was first used to outline comet traces within the imaged area, and kymographs were generated for selected traces using the Kymograph plugin for ImageJ from J. Rietdorf (Friedrich Miescher Institute, Basel, Switzerland) and A. Seitz (EMBL, Heidelberg, Heidelberg, Germany).

Quantitative Analysis of +TIP Density in Fixed Cells—Immunostaining in cultured myotubes was performed as described previously (13). The AChR cluster was defined as a region of interest (ROI), and the total number of EB3 comets were counted using ImageJ. A similar ROI was selected outside the cluster for each cell, and EB3 comets were counted within this as well. The number of comets per unit area was then calculated inside and outside the clusters to obtain EB3 comet density. Intensity profiles for GFP and EB3 immunostainings were generated for the corresponding single channel images, using the Plot Profile tool in ImageJ, after defining the GFP signal from each plus-end as a segmented line ROI.

Estimation of AChR Delivery Versus Removal from Changes in Size and Density of AChR Clusters—Changes in AChR insertion into clusters in response to pharmacological or genetic manipulation of myotubes were inferred from changes in AChR cluster size. In principle, changes in agrin-induced AChR cluster size in response to such treatments might occur through changes of AChR insertion into, or AChR removal from, the clusters. These possibilities can be distinguished from one another by employing appropriate experimental protocols (13). Specifically, changes in cluster size of AChRs stained before the treatment will reveal changes in AChR removal, whereas changes in the size of clusters stained after the treatment will reflect changes in AChR insertion, on the condition that the density of the AChRs in the cluster remains unchanged.

To analyze the effect of constitutive GSK3β on AChR clustering, 24–36 h after switching to differentiation medium, myotubes were transduced with adenoviral particles encoding mRFP-GSK3β-S9A and 48–72 h later were fixed in 2% PFA for 5 min. Cells were stained for AChR clusters using α-BTX-Alexa647, whereas mRFP signal was imaged unstained, using intrinsic protein fluorescence. Images were taken at low magnification (HC Plan Apo ×20/0.70 objective; inverted microscope (DMI 6000B; Leica); 1394 ORCA-ERA camera (Hamamatsu Photonics), Volocity 6.0.1 (PerkinElmer Life Sciences)), and the AChR cluster area was quantified using ImageJ. For each experiment, all conditions were imaged under identical settings within the same imaging session. Cultures within one experiment were cultured on the same batch of COS-agrin dishes (see under "Preparation of Primary Muscle Cultures" above). The size of the AChR cluster was defined by drawing an ROI using ImageJ, and the integrated fluorescence density was divided by the ROI to obtain AChR cluster density. A corresponding region within the same myotube was outlined as an ROI for each cluster to subtract background fluorescence. Outlining the ROI by hand was preferred to using thresholding in ImageJ, because on many myotubes it allowed us to include clusters with magnetic beads (originating from the myoblast purification) in their vicinity whose autofluorescence interfered with automatic thresholding; defining the ROI manually thus allowed us to increase sample size. Manual definition of the ROI was validated by comparing the results with those from automatic thresholding in bead-free myotubes. The results with the two methods are quantitatively similar. It is important to note that because the COS-agrin dishes were freshly prepared for each myotube culture, the size and density of the agrin patch (and therefore the size and density of AChR clusters) varied considerably across experiments depending on the efficiency of transfection and secretion of agrin. It was therefore not useful to calculate absolute sizes and densities. Instead, values were calculated relative to the control, and normalized values were averaged over the various experiments.

To analyze the effect of constitutive GSK3β on AChR clustering with and without the GFP-CLASP2 mutants, 24–36 h after switching to differentiation medium, myotubes were transduced with the indicated adenoviral constructs, and 48–72 h later were fixed in 4% PFA for 5 min. Cells were stained

for AChR clusters using α-BTX-Alexa647. GFP and mRFP signals (from GFP-CLASP2 and mRFP-GSK3β-S9A, respectively) were imaged unstained, using intrinsic protein fluorescence. Images were taken at low magnification using an SPE confocal scanning laser microscope (DMI 4000B; Leica) at a resolution of 1024 × 1024 pixels and ×20 magnification. AChR cluster area was quantified using ImageJ.

RESULTS

Rescue of AChR Cluster Size in Clasp2 Knock-out Myotubes by Overexpression of Wild Type GFP-CLASP2—RNA sequencing has revealed that in the muscle and neuromuscular junction only *Clasp2*γ mRNA is expressed (data not shown), which encodes an ~140-kDa isoform of CLASP2 (14). Recently, GFP-tagged CLASP2 constructs have been described, in which potential GSK3 phosphorylation sites were mutated either to alanine (CLASP2–9XS/A) or to aspartic acid (CLASP2–8XS/D), giving rise to phospho-resistant and phosphomimetic forms of CLASP2, respectively (20). Compared with a nonmodified form of CLASP2, these proteins were shown to bind MTs and MT ends with different characteristics in cultured keratinocytes. However, these CLASP2 proteins (CLASP2–9XS/A, CLASP2–8XS/D, and CLASP2-WT) lack part of the N terminus of CLASP2γ, including a TOG-like domain (28), which has been suggested to contribute to the binding of CLASP to MTs (19).

Using primary myotubes cultured on a laminin substrate locally impregnated with agrin (see "Experimental Procedures") (13) as an *in vitro* two-dimensional model for AChR clustering and density, we could show previously that myotubes derived from *Clasp2* knock-out mice have reduced AChR cluster size through reduced AChR insertion (13). To ascertain that the function of GFP-tagged wild type CLASP2 in AChR clusters is not affected by N-terminal truncation, we tested whether it was functional in our system and could rescue the *Clasp2* knock-out phenotype on AChR clustering in myotubes. We infected myotubes with truncated wild type GFP-CLASP2 and compared AChR cluster size and density in these cultures with noninfected myotubes derived from wild type or *Clasp2* knock-out mice. Myotubes analyzed were selected visually based on the expression of the appropriate constructs and their respective markers. Expression of truncated GFP-CLASP2 rescued the cluster area defect in the *Clasp2* knock-out myotubes (Fig. 1, *A* and *B*), suggesting that this form of CLASP2 is functional in myotubes.

We previously described that addition of soluble neural agrin to myotube cultures causes the rapid phosphorylation of GSK3 (13). Our hypothesis predicts that agrin, through local inactivation of GSK3β, dephosphorylates CLASP2, thus promoting its binding to MT plus-ends at the cluster (13). Using wild type GFP-CLASP2 accumulation as a read-out for CLASP2 dephosphorylation by agrin, we examined the time course of GFP-CLASP2 accumulation at AChR clusters by culturing myotubes expressing wild type GFP-CLASP2 on laminin alone (*i.e.* without agrin patches), and we observed the accumulation of GFP over time in response to added agrin at laminin-induced AChR clusters, which do form at low incidence in the absence of agrin (29). Before adding soluble agrin to the culture medium, no

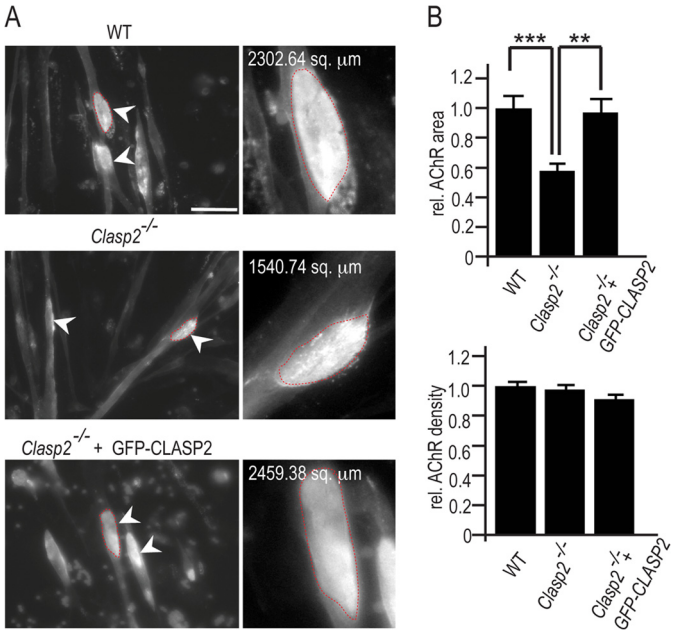

FIGURE 1. **Expression of GFP-CLASP2 rescues the decrease in cluster size of *Clasp2* knock-out myotubes.** *A,* representative AChR clusters induced in cultured myotubes by local deposits of neural agrin in the culture substrate. Primary myotubes isolated from wild type (*WT*) and *Clasp2* knock-out (*Clasp2*$^{-/-}$) mice were either cultured as such or infected with adenovirus expressing GFP-CLASP2, and 2 days later, AChR clusters were stained with α-BTX-Alexa594. Representative images of AChR clusters are shown in WT, *Clasp2*$^{-/-}$, and *Clasp2*$^{-/-}$ plus GFP-CLASP2 myotubes (*scale bar,* 105 μm). *Arrowheads* point to AChR clusters, and the representative cluster outlined in *red* is enlarged in the adjacent panel with the area indicated in μm^2. *B,* quantification of AChR cluster area and density. *Graphs* depicting relative AChR cluster size (*upper panel*) and AChR density (*lower panel*) show mean ± S.E. $n = 41$ control, 49 *Clasp2*$^{-/-}$, and 33 *Clasp2*$^{-/-}$ plus GFP-CLASP clusters; **, $p < 0.001$; ***, $p < 0.0001$; two-sided *t* test.

GFP-CLASP2 accumulation was seen (Fig. 2). Clear GFP fluorescence was detected 4 h after addition of soluble agrin (Fig. 2), and the fluorescence increased in intensity over the next 18 h. This indicates that truncated GFP-CLASP2 is properly activated by agrin. Interestingly, its recruitment to clusters lags somewhat behind the time course of phosphorylation of GSK3β demonstrated earlier (13). Taken together our data suggest that the truncated wild type, phospho-resistant, and phosphomimetic forms of CLASP2 can be used in our studies to examine the role of GSK3-dependent CLASP2 phosphorylation in the regulation of agrin-induced MT capturing and AChR cluster size and density.

Rescue of AChR Cluster Size in Myotubes Expressing Constitutively Active GSK3β by Expression of Phospho-resistant GFP-CLASP2—Mammalian CLASP2 contains multiple S*XXX*S repeat GSK3 phosphorylation motifs within the central, intrinsically disordered protein domain surrounding the two CLASP2 S*X*IP EB1-binding motifs (18). CLASP2 interactions, either directly with MTs or with growing MT ends through EB1, are controlled by GSK3 (20). Multisite phosphorylation of these S*XXX*S motifs occurs by the action of a priming kinase, which phosphorylates a first site, followed by the rapid and processive GSK3-mediated phosphorylation of all other sites. This inhibits MT binding through disruption of distributed electrostatic interactions (18). Indeed, the previously generated CLASP2 construct in which all nine of the potential GSK3

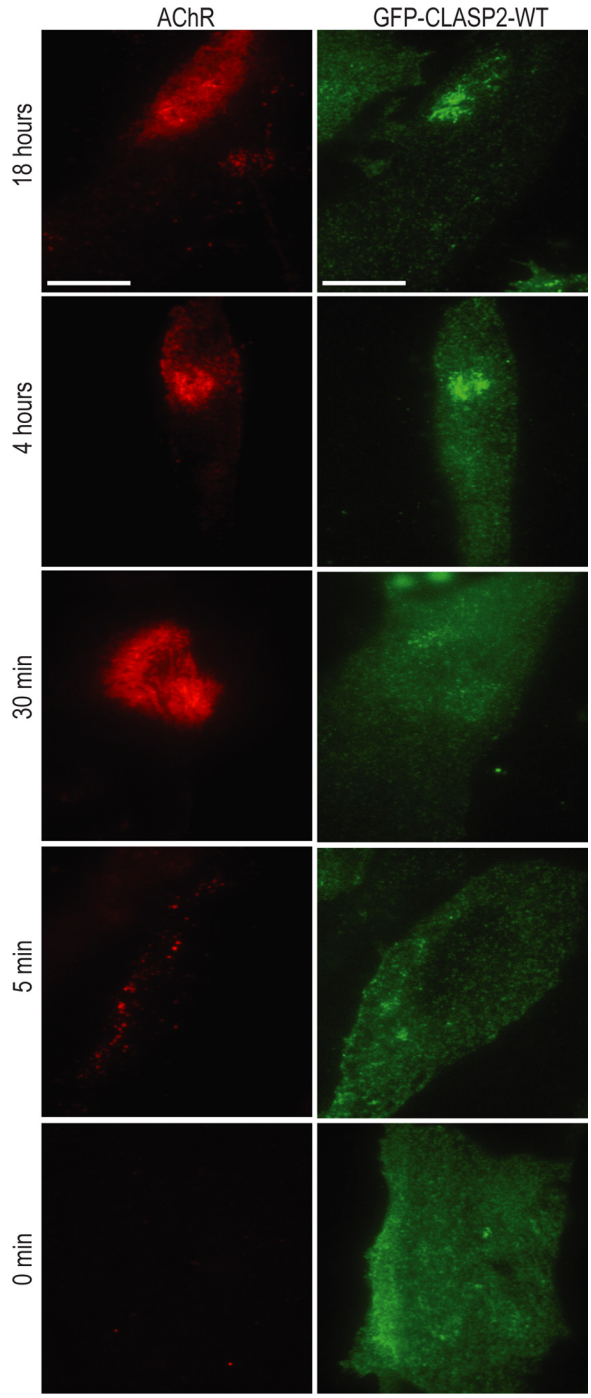

FIGURE 2. **Time course of GFP-CLASP2 accumulation at AChR clusters.** Primary myotubes cultured on laminin were infected with GFP-CLASP2. Two days later, cultures were treated with 10 nM soluble agrin for the indicated times, before fixing in 2% PFA. α-BTX-594 was added to cells after fixation. Cells were imaged using TIRF microscopy. Note the accumulation of GFP-CLASP2 at AChR clusters at 4 and 18 h after agrin addition. *Scale bar,* 10 μm.

phosphorylation sites are mutated to nonphosphorylatable alanine residues (CLASP2–9XS/A) strongly enhances binding to MTs and EB1 in cultured cells, whereas the CLASP2 construct in which the eight serine residues that we confirmed to be phosphorylated are mutated into negatively charged phosphomimetic aspartate residues (CLASP2–8XS/D), completely disrupts MT binding.

We have shown previously that inactivation of GSK3 by the inhibitor CHIR99021 renders the AChR cluster area larger in wild type myotubes but is unable to rescue the cluster size defect in *Clasp2* knock-out myotubes (13). These results suggested that GSK3 activity is an important parameter controlling AChR cluster size and that GSK3 acts, at least in part, through CLASP2. To provide further evidence for agrin promoting AChR insertion through MT capture via GSK3β-dependent-CLASP2 dephosphorylation, we tested for an effect of GSK3β activity on AChR clustering. We compared agrin-induced AChR clusters, which were stained with α-BTX-Alexa647, in untreated wild type myotubes with those in wild type myotubes induced to express constitutively active GSK3β (*i.e.* mRFP-GSK3β-S9/A (20)), both in the absence and in the presence of the CLASP2 phospho-resistant mutant (GFP-CLASP2–9XS/A). We found that expression of mRFP-GSK3β-S9/A alone reduced AChR cluster size (Fig. 3, *A* and *B*). When, in addition to mRFP-GSK3β-S9/A, GFP-CLASP2–9xS/A was expressed, the reduction of cluster size was reversed (Fig. 3, *A* and *B*). The quantitative effect of the introduced constructs on AChR cluster size depended on their respective expression levels. For example, in experiments where the level of mRFP-GSK3β-S9/A was lower, the reduction in cluster size was lower, but GFP-CLASP2-WT partially rescued cluster size, and the rescue by GFP-CLASP2–9XS/A was more pronounced (data not shown) than illustrated in Fig. 3. These data suggest that a reduction in AChR cluster size due to overactive GSK3 is overcome by expression of a phosphorylation-resistant form of CLASP2 but not of wild type CLASP2. Thus, one way for agrin to regulate AChR clustering is by inactivation of GSK3β, which increases the local content of nonphosphorylated CLASP2, thereby promoting MT capture at, and as a consequence AChR delivery to, the cluster.

Dynamic Behavior of GFP-tagged CLASP2 Proteins in Myotubes—To observe the dynamic behavior of wild type and mutant GFP-CLASP2, we infected cultured myotubes with adenoviral constructs expressing the different proteins, stained AChR clusters with α-BTX-Alexa-594, and performed time-lapse TIRF microscopy experiments. Outside AChR clusters in myotubes expressing phosphomimetic CLASP2, GFP-CLASP2–8XS/D-positive MT plus-ends could barely or not at all be resolved, consistent with the strongly reduced binding of mutant CLASP2 to MT plus-ends (Fig. 4, *A* and *B*). In contrast, in myotubes expressing CLASP2–9XS/A examined at identical settings, comets were visible, which appeared quite bright, consistent with a high affinity of CLASP2–9xS/A for MT plus ends (Fig. 4, *C* and *D*). Inside the agrin-induced AChR clusters of myotubes expressing GFP-CLASP2–8XS/D, the GFP fluorescence was very bright and immobile, and it appeared either striped or unstructured (Fig. 4, *A* and *B*). A similar pattern was observed in myotubes expressing GFP-CLASP2–9xS/A, except that signals within the AChR cluster resembled comet-like structures more often (Fig. 4, *C* and *D*).

Neither CLASP2–8XS/D nor GFP-CLASP2–9XS/A GFP fluorescence at AChR clusters showed much dynamic behavior over time, as seen from the complete superposition of the fluorescence signals from single frames and from maximum inten-

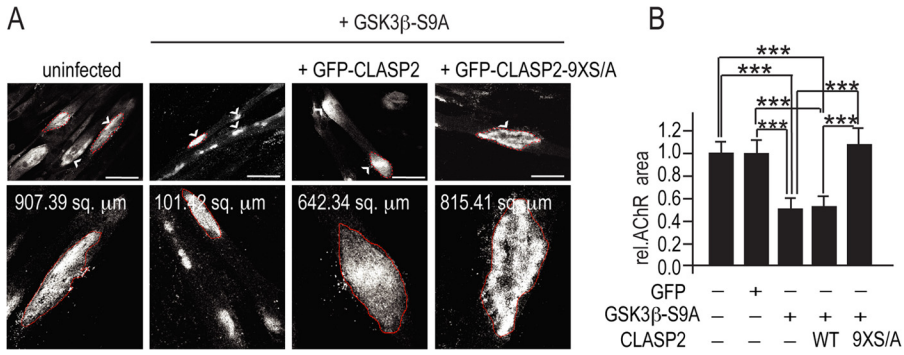

FIGURE 3. **Agrin-induced AChR clustering in myotubes is inhibited by forced expression of constitutively active GSK3β (mRFP-GSK3β-S9A) and is rescued by expression of phosphorylation-resistant CLASP2.** *A,* representative AChR images on cultured myotubes. Myotubes were cultured under the conditions described in Fig. 1. All *scale bars,* 50 μm. *Arrowheads* indicate AChR clusters. A representative AChR cluster from each image is outlined in *red* and enlarged in the *lower panels*. *Numbers* indicate the corresponding AChR area in μm^2. *B,* quantification of AChR cluster area. Myotubes differentiated on patches of immobilized neural agrin were infected with adenoviral vectors coding for either GFP, mRFP-GSK3β-S9A, or a combination of mRFP-GSK3β-S9A and either wild type (*WT*) CLASP2 or phosphorylation-resistant CLASP2–9xS/A. Two days later, myotubes were fixed in PFA and stained for AChRs with α-BTX647, and relative AChR cluster size was quantified. *Graphs* show means ± S.E. ***, $p < 0.001$; for two-sided *t* test; *n* (uninfected) = 48; *n* (GFP) = 60; *n* (GSK3β-S9A infected) = 56; *n* (GSK3β-S9A and CLASP2-WT infected) = 47, and *n* (GSK3β-S9A and CLASP2–9xS/A infected) = 36.

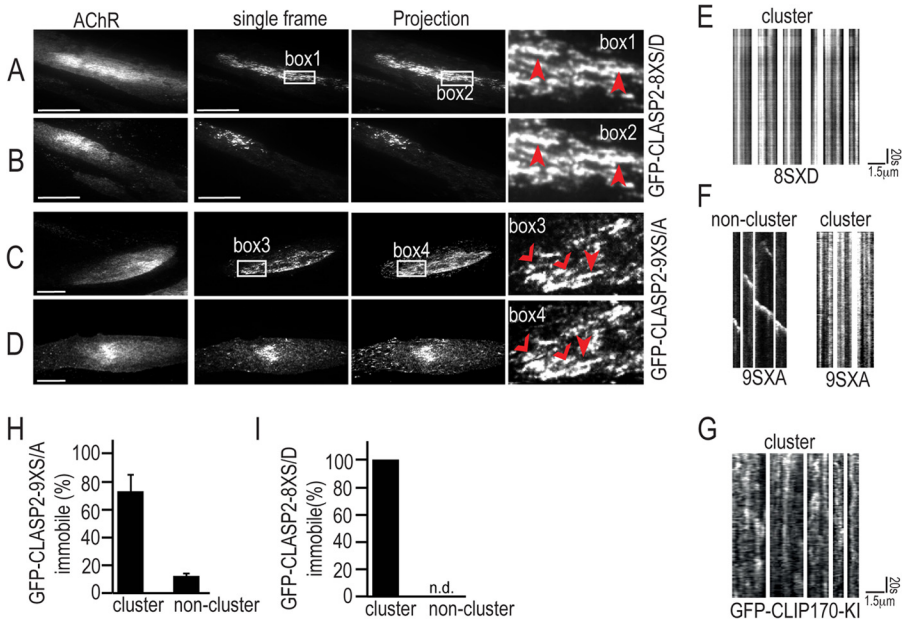

FIGURE 4. **Phosphomimetic (CLASP-8xS/D) and phosphorylation-resistant (CLASP2–9xS/A) GFP-CLASP2 mutants accumulate at agrin-induced AChR clusters.** *A–D,* representative AChR or GFP images in cultured myotubes. Myotubes differentiated on patches of immobilized neural agrin were infected with adenoviral vectors coding for GFP-tagged phosphomimetic (CLASP-8xS/D) (*A* and *B*) or phosphorylation-resistant CLASP2–9XS/A (*C* and *D*). Panels marked *Projection* are maximum intensity projections of 160–180 frames taken in TIRF microscopy at 1 frame/s. Note that in myotubes expressing GFP-CLASP2–8XS/D, fluorescent protein accumulations cannot be clearly observed outside the AChR clusters, in contrast to myotubes expressing GFP-CLASP2–9XS/A. Inside clusters, most GFP signals appear *striped* (*enlarged boxes 1–4, closed arrowheads*) or punctate (*enlarged boxes 3* and *4, open arrowheads*); only a few signals in GFP-CLASP2–9xS/A-expressing myotubes are mobile. The striped GFP fluorescence signals show no dynamics as shown from the similarity of single frames with projections of 160 frames (*insets*) in *A* and *C*. *Scale bars,* 10 μm. *E–G,* kymograph analysis and relative mobility of GFP-CLASP2. Kymographs were obtained from GFP signals in myotubes expressing the respective mutants as indicated. Kymographs from AChR clusters in GFP-CLIP-170-expressing myotubes derived from GFP-CLIP-170 knock-in (*KI*) mice (13) are shown for comparison (*G*). *H* and *I,* quantification of relative GFP-CLASP2 mobility (*i.e.* the percentage of immobile spots) from GFP-CLASP2–8XS/D- and GFP-CLASP2–9XS/A-expressing myotubes. *Graphs* show means ± S.E. GFP-CLASP2–8XS/D, 55 signals analyzed from three cells; GFP-CLASP2–9XS/A, 156 signals analyzed from three cells.

sity projections of multiple frames (Fig. 4, *A* and *C*, and *boxed insets*). Some of these had a shorter, more punctate appearance (*box 3* and *4, open arrowheads*) than the comet-like GFP signals (*box 3* and *4, closed arrowheads*). Both types resulted in "static kymographs" of relatively constant intensity over time (Fig. 4, *E, F, H,* and *I*). This was in contrast to the GFP signals in myotubes derived from GFP-CLIP-170 knock-in mice (13), where GFP fluorescence along kymographs varied in intensity over time (Fig. 4*G* derived from Ref. 13). Strikingly, GFP-CLASP2–8XS/D, which binds MT ends with reduced affinity (20), displayed a completely static behavior in AChR clusters (Fig. 4*E*). Because the majority of the GFP-CLASP2–8XS/D-positive patterns inside clusters are unlikely to represent captured MTs, we attributed fluorescence at AChR clusters to binding of the GFP-CLASP2 mutant to other proteins, for example to LL5β, which is enriched at agrin-induced AChR clusters (23), and which is relatively immobile, at least in cortical regions of cultured fibroblasts (22). Taken together, our data suggest that the binding of CLASP2 to MTs inside clusters renders the protein more dynamic.

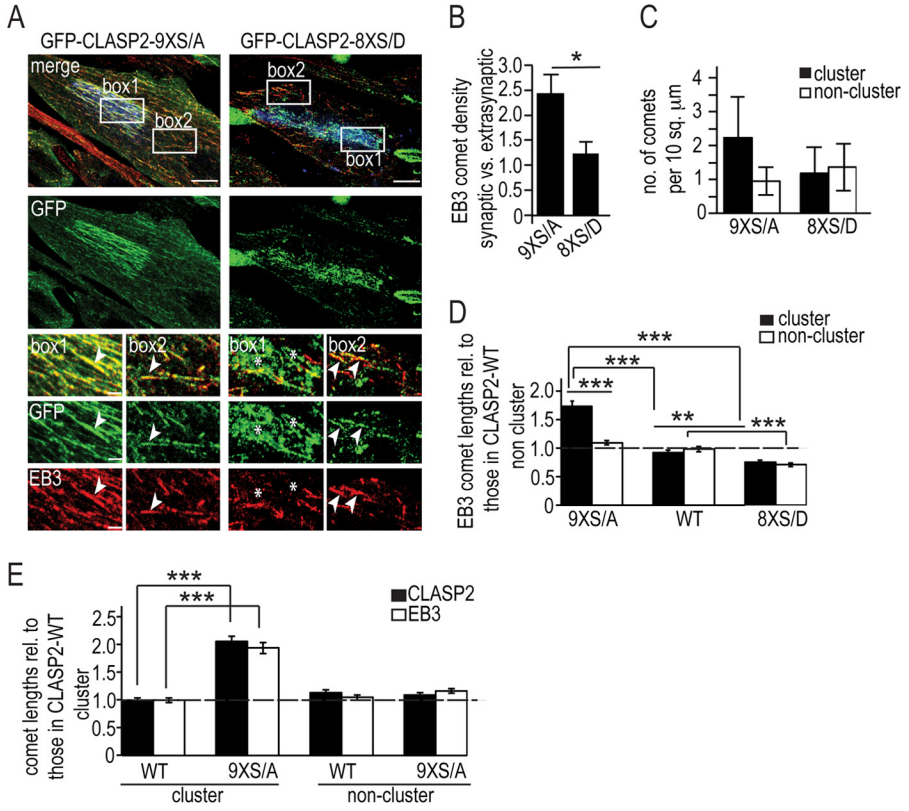

FIGURE 5. **Overexpression of CLASP2 affects MT behavior at agrin-induced AChR clusters.** *A,* representative immunofluorescent stainings in cultured myotubes. Myotubes were infected with GFP-tagged phosphorylation-resistant CLASP2–9XS/A (*left panels*) or phosphomimetic CLASP-8XS/D (*right panels*). Two days later, myotubes were fixed and stained for AChRs with α-BTX-Alexa647 (*blue*), GFP (CLASP mutant, *green*), and EB3 (*red*) and examined by CLSM. *Boxes* show areas enlarged in *bottom panels* (*boxes 1*, inside; *boxes 2*, outside AChR cluster). Note the unstructured GFP immunoreactivity at clusters of myotubes expressing phosphomimetic CLASP2 (see text for discussion). *Arrowheads* indicate comets positive for EB3 and CLASP2; *asterisks* indicate GFP-CLASP2 staining in the absence of EB3 co-localization. *Scale bar,* 10 μm; 2.5 μm (*inset*). *B,* quantification of MT plus-end densities. Myotubes were infected, fixed, and stained as described in *A*. EB3-coated MT plus-ends were measured inside and outside clusters. Densities were calculated by dividing the number of MT plus-ends by respective areas (means ± S.E.; $n = 8$ clusters examined in CLASP2–9XS/A, $n = 7$ clusters examined in CLASP2– 8xS/D, from two independent experiments). *, $p < 0.05$; two-sided *t* test. *C,* number of comets per unit area in CLASP2–9XS/A and CLASP2– 8XS/D-expressing myotubes. Note that number of comets at the cluster is increased in 9XS/A compared with extrasynaptic areas. This increase is abolished upon 8XS/D expression. *Bars* give mean ± S.D. from $n = 4$ cells each. *D,* quantification of EB3-decorated MT plus-end lengths. Myotubes, infected with GFP-tagged wild type (*WT*), phosphorylation-resistant, or phosphomimetic CLASP2, were fixed and stained as described in *A*. The length of fluorescent EB3 "comets" on MT plus-ends was measured. *Graphs* show means ± S.E. Six cells were analyzed per construct; total number of comets analyzed = 226 for GFP-CLASP2–9XS/A; 183 for GFP-CLASP2-WT; and 186 for GFP-CLASP2– 8XS/D. *E,* quantification of EB3- or CLASP2-decorated MT plus-end lengths. Myotubes, infected with GFP-tagged wild type (*WT*) or phosphorylation-resistant (9XS/A) CLASP2, were fixed and stained as described in *A*. The length of fluorescent EB3 or CLASP2 signal on MT plus-ends was measured inside and outside clusters. A total of 726 comets were analyzed; 430 for CLASP2–9XS/A from six cells; 296 for CLASP2-WT from three cells. *Graphs* show means ± S.E. **, $p < 0.01$; ***, $p < 0.001$, two-sided *t* test. Comet lengths were normalized as shown. CLASP2 lengths in WT noncluster are from three cells only, as in CLASP2-WT-expressing cells, and CLASP2 comets outside the cluster were difficult to distinguish from background.

Configuration of Captured MTs at AChR Clusters—At the leading edge of migrating cells, the MTs are captured depending on the phosphorylation state of CLASP2 (14–16, 20). When nonphosphorylated, CLASP2 binds to MT plus-ends and thus mediates MT capture to the cell cortex. To examine whether CLASP2-dependent MT capturing at agrin-induced AChR clusters depends on the CLASP2 phosphorylation state, we compared MT plus-end density at clusters in myotubes either expressing GFP-CLASP2–9XS/A or GFP-CLASP2– 8XS/D. We visualized plus-ends of dynamic MTs independently of their CLASP2 binding in fixed myotubes by staining them with an antibody to EB3, the core +TIP expressed in cultured myotubes (13). AChRs were stained with α-BTX-Alexa647. Indeed, enrichment of EB3-decorated MT ends was seen at agrin-induced AChR clusters in myotubes expressing GFP-CLASP2–9XS/A but not GFP-CLASP2– 8XS/D (Fig. 5, *A–C*).

Conspicuously, in myotubes expressing GFP-CLASP2–9XS/A, EB3-stained comets were significantly longer than in myotubes expressing GFP-CLASP2-wild type or GFP-CLASP2-8XS/D (Fig. 5, *A* and *D*), particularly in MTs inside AChR clusters. Interestingly, binding of both EB3 and GFP-CLASP2–9xS/A to MTs increased markedly (Fig. 5*E*). This is consistent with GFP-CLASP2–9xS/A binding to MTs and attracting EB3 to these MTs. To visualize this more directly, we measured fluorescent intensities of GFP-CLASP2 (WT and 9XS/A) and EB3 along MT ends inside and outside clusters. We found that in all situations EB3 staining was co-extensive with GFP-CLASP2, but in the presence of CLASP2–9XS/A EB3 comets were longer, particularly inside the clusters (Fig. 6*A*).

The length of EB3 comets inside clusters of GFP-CLASP2–9XS/A-expressing cells, as measured by standard confocal microscopy (CLSM) in antibody-stained fixed cells (on average 4.5 μm, Fig. 6*A*), is considerably larger than the length of GFP-CLIP-170- or GFP-CLASP2–9XS/A-positive signals inside clusters, as measured with TIRFM in live cells (on average 1.5 and 2 μm, respectively, Fig. 6*B*). These data indicate that +TIP-

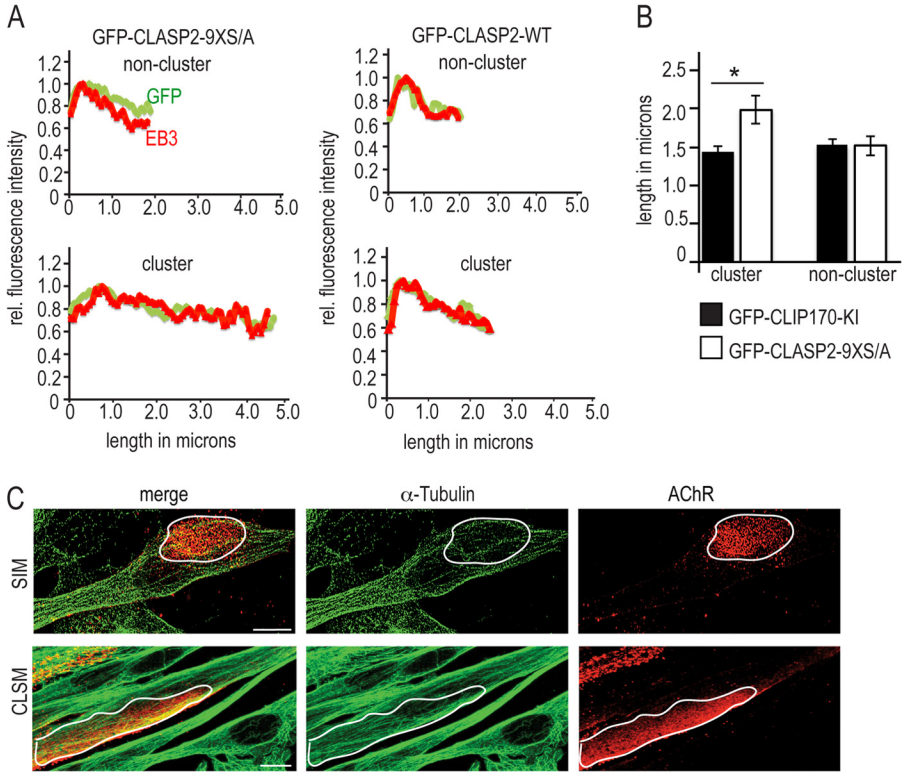

FIGURE 6. **Intensity profiles of GFP and EB3 immunostaining in primary myotubes infected with CLASP2-expressing adenoviral constructs.** *A,* myotubes infected with GFP-tagged wild type (*WT*) or phosphorylation-resistant (9S/A) CLASP2 were fixed and stained for AChRs, GFP (*green*), and EB3 (*red*) and examined by CLSM. Relative intensity profiles of GFP and EB3 immunostaining are shown, with average of three cells per condition; a total of 53 profiles were analyzed in GFP-CLASP2–9XS/A and 65 profiles in GFP-CLASP2-WT. *B,* lengths of comets analyzed from TIRFM images as depicted in Fig. 3 in myotubes infected with GFP-CLASP2–9XS/A and in GFP-CLIP170-KI myotubes. *n* (GFP-CLIP170) = 23 comets; *n* (GFP-CLASP2–9XS/A) = 26 comets; *, $p < 0.05$. *C,* SIM and CLSM images of α-tubulin immunostaining (*green*) with AChRs (*red*) in primary myotubes. *Upper panel,* maximum intensity projections of three slices in an image stack acquired in SIM at a step size of 140 nm. *Scale bar,* 10 μm. *Lower panel,* maximum intensity projection of two slices in an image stack acquired in CLSM at a step size of 300 nm. *Scale bar,* 7.5 μm.

coated MT plus-ends are not anchored parallel to the plasma membrane of the AChR cluster but under an angle. This causes loss of part of the GFP signal at plus-ends in experiments that use TIRFM. In fact, some of the immobile punctae of GFP-CLASP2–9XS/A (or GFP-CLIP-170; see Fig. 4) might represent captured MT plus-ends anchored perpendicular to the membrane. Interestingly, the MT network appeared to be organized parallel to the AChR membrane when visualized with high resolution SIM and with CLSM, and we did not find an increased MT density inside clusters, as compared with outside clusters (Fig. 6*C*), despite the increased density of +TIP-coated MT plus-ends (Fig. 5, *A*–*C*)[5] and the increase in immobile GFP signals. The apparent discrepancy in the ratio of MTs and MT plus-ends inside and outside a cluster is explained by the fact that outside clusters MTs are more dynamic as many MTs will be shrinking and will not have an end that is stained with EB3. By contrast, inside the cluster most MTs are stable or growing, and all of these have EB3 at their ends. Furthermore, our data indicate that some of the immobile GFP-CLASP2- or GFP-CLIP-170-positive dots inside clusters either represent contacts between the MT lattice and proteins at the cluster membrane or represent proteins that are not bound to MTs.

MT Plus-end Density and AChR Cluster Size Are Correlated—According to our hypothesis, MT capture serves to deliver AChRs to the synaptic membrane of the NMJ (13). Given the inverse relation of CLASP2 phosphorylation to MT binding affinity (20), AChR delivery (and thus cluster size) would be expected to be inversely related to the abundance of phosphorylated CLASP2. We tested for an effect of CLASP2 phosphorylation state by comparing agrin-induced AChR cluster sizes, stained with α-BTX-Alexa647, in untreated wild type myotubes with those in wild type myotubes induced to express wild type GFP-CLASP2, phosphomimetic GFP-CLASP2–8XS/D, or nonphosphorylatable GFP-CLASP2–9XS/A. Myotubes analyzed were again selected visually based on the expression of the appropriate constructs and α-BTX-Alexa647.

In agreement with our hypothesis, and consistent with the density of EB3 comets at the agrin-induced AChR clusters, cluster size correlated inversely with the abundance of nonphosphorylated CLASP2 (Fig. 7, *A* and *B*, and Table 1). Specifically, clusters were largest in myotubes expressing nonphosphorylatable GFP-CLASP2–9xS/A and smallest in myotubes expressing phosphomimetic GFP-CLASP2–8xS/D (Fig. 7, *B* and *C*); in contrast, AChR densities were not affected by the type of CLASP2 mutant expressed (Fig. 7, *D* and *E*). Therefore, the changes of cluster size observed indicate a direct effect of the mutants on AChR insertion because the stability of AChRs remains unchanged. Interestingly, expression of GFP-tagged wild type CLASP2 increased AChR cluster size (albeit nonsignificantly) compared with noninfected cells (Fig. 7*C*). Com-

[5] S. Basu, S. Sladecek, H. R. Brenner, and N. Galjart, unpublished observations.

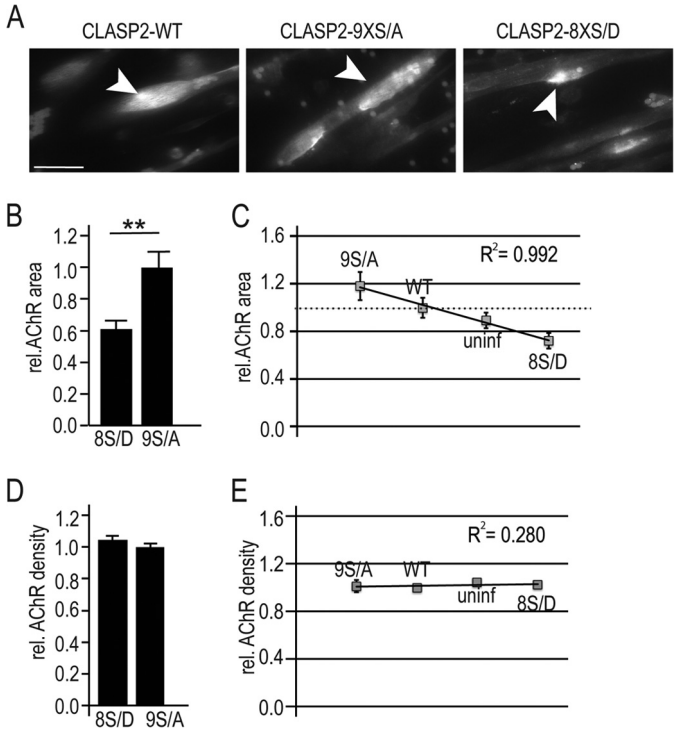

FIGURE 7. **AChR cluster size increases in proportion to the amount of available (active) CLASP2.** *A,* representative images of agrin-induced AChR clusters in cultured myotubes. Primary myotubes differentiated on patches of immobilized neural agrin were infected with adenoviral vectors coding for GFP-tagged wild type CLASP2 (CLASP2-WT), phosphorylation-resistant CLASP2 (CLASP2–9XS/A), or phosphomimetic CLASP2 (CLASP2–8XS/D). *Scale bar,* 100 μm. *B* and *C,* relative AChR cluster size in myotubes expressing indicated constructs. Cluster area was normalized to GFP-CLASP2–9XS/A in *B*. *C*, relative AChR cluster sizes (means ± S.E.) in myotubes expressing indicated constructs were plotted as a scatter with the regression coefficient indicated in the respective graphs and normalized to GFP-CLASP2-WT. **, $p < 0.001$, two-sided *t* test. $n = 75$ WT, 76 9XS/A, 59 8XS/D, and 41 uninfected clusters, two independent experiments. *D* and *E,* relative AChR density in the same myotubes as above expressing indicated constructs. Similarity of relative AChR densities at same clusters as in *B* and *C* excludes changes in AChR stability as the cause for differences in cluster size. Thus, changes in cluster size indicate changes in AChR insertion.

bined, these data indicate that agrin-induced MT density and AChR cluster size are correlated both with CLASP2 phosphorylation at the cluster and by the levels CLASP2.

DISCUSSION

This study adds a new mechanism for agrin to organize sharply delineated clusters of high AChR density at the NMJ. In addition to trapping AChRs through the agrin-induced postsynaptic apparatus (11), the CLASP2-mediated MT capturing to synaptic clusters contributes substantially to the size of agrin-induced synaptic AChR clusters.

Two lines of evidence support the involvement of focal GSK3β inactivation and, as a consequence, the phosphorylation state of CLASP2 in synaptic AChR delivery by synaptic MT capturing. First, the enrichment of MT plus-ends visualized by EB3 staining at AChR clusters in myotubes expressing wild type or GFP-CLASP2–9XS/A is absent when phosphomimetic GFP-CLASP2–8XS/D is expressed. Interestingly, cluster size is increased in GFP-CLASP2–9XS/A- compared with GFP-CLASP2–8XS/D-expressing myotubes. Second, AChR cluster size is reduced by constitutively active GSK3β (GSK3β-S9A), an effect that is rescued by GFP-CLASP2–9XS/A, which is resistant to phosphorylation by GSK3β in its MT plus-end tracking domain. These data suggest that GSK3β regulates AChR delivery by controlling CLASP2 phosphorylation state and MT capture.

Using next generation sequencing on RNA derived from muscle or the NMJ, we have recently shown that in these tissues only one isoform of CLASP2, called CLASP2γ, is expressed (data not shown). This isoform of ~140 kDa is shorter than the CLASP2α isoform of ~160 kDa that is present in most cell types. CLASP2α has three TOG-like domains (31). CLASP2γ lacks the most N-terminal TOG-like domain that is found in CLASP2α. Compared with CLASP2γ, the N-terminally truncated CLASP2 wild type construct used in our studies, which rescued AChR cluster size in *Clasp2* knock-out myotubes, also lacks the middle TOG-like domain. The function of this second TOG-like domain is not yet well defined. It may contribute to MT binding to some extent (19); however, we have shown previously that this is mostly mediated by a third TOG-like domain C-terminal to the disordered central part of the protein (15, 19, 33), which is present in the rescue construct. Overexpression of the rescue construct may compensate for a slightly reduced MT binding due to the absence of the second TOG-like domain.

Conspicuously, both GFP-CLASP2–9XS/A and GFP-CLASP2–8XS/D were enriched at agrin-induced AChR clusters, although for the latter, *i.e.* phosphomimetic CLASP2, the enrichment could not have been due to MT capturing. Thus, the enrichment of overexpressed GFP-CLASP2–8XS/D occurred through a different mechanism. We hypothesize this might be through binding to LL5β, as this protein is enriched at NMJs *in vivo* (23), and CLASP2 can associate with the cell cortex and with LL5β independently of its binding to MTs (17, 22, 30). In addition, we have observed that overexpression of the LL5β-binding CLASP2 C terminus abolishes MT capture at AChR clusters.[5] We explain this by assuming that overexpression titrates out the endogenous LL5β-CLASP2 interaction. Alternatively, overexpression of the CLASP2 C terminus may affect the interaction of the C terminus of CLASP2 with another protein at the cluster.

Combined with our previous findings (13), the present experiments strongly suggest that agrin promotes the delivery of AChRs (and possibly other synapse-specific molecules) to the synaptic muscle membrane through the local inactivation of GSK3β; in turn, this maintains CLASP2 in a dephosphorylated state near the synaptic membrane. As a consequence, CLASP2 will accumulate on plus-ends of dynamic MTs as they approach the synaptic region, thus enabling CLASP2-mediated MT capturing at the cluster membrane. We have shown increased EB3 density and comet length in AChR cluster regions in CLASP2–9XS/A-expressing cells, suggesting that more MTs are captured in these cells and that MTs are more stable and immobile, compared with uninfected cells. However, EB1 has been shown to catalyze turnover of its own binding sites on MT ends thereby increasing the chances of catastrophe (32). On the basis of these results, one would expect that increased MT end-binding by EB3, which is very similar to EB1, should increase MT dynamicity. That the opposite occurs is explained by assuming that stable MT ends at the NMJ have a

TABLE 1

AChR cluster size and density in GFP-CLASP2-WT-, GFP-CLASP2–9SXA-, and GFP-CLASP2– 8SXD-infected myotubes

AChR cluster sizes and densities (means ± S.D.) obtained from two independent experiments (Exp. 1 and 2) show the correlation of AChR cluster size with CLASP2 phosphorylation. Note that cluster sizes and densities vary between the two experiments, yet the correlation is maintained. AU is arbitrary units.

Exp.		WT	9XS/A	8XS/D	Uninfected
1	AChR size (μm^2)	938.45 ± 697.53	1144.13 ± 882.02	759.10 ± 529.93	874.34 ± 509.77
1	AChR density (mean intensity (AU)/(μm^2))	136.33 ± 15.89	139.88 ± 20.91	150.06 ± 26.85	144.40 ± 17.79
2	AChR size (μm^2)	344.27 ± 182.08	385.88 ± 222.17	204.86 ± 124.39	301.79 ± 158.13
2	AChR density (mean intensity (AU))/(μm^2)	74.08 ± 13.24	61.04 ± 10.74	68.09 ± 14.97	73.38 ± 14.55

high CLASP2–9XS/A (or nonphosphorylated CLASP2) to EB3 ratio; in this case CLASP2 stabilizes the MT end and attracts EB3. By contrast, on a growing MT end, EB3 attracts CLASP2, and the ratio of nonphosphorylated CLASP2 to EB3 is too low for CLASP2 to stabilize the MT end.

Our data further suggest that not only the phosphorylation state of CLASP2 but also the amount of protein determine how many MTs can be captured. Thus, CLASP2 is a limiting factor in the capture of MTs at the NMJ and in determining AChR cluster size. In addition, we propose that not only MT plus-ends are anchored to the membrane but that some of the immobile and punctate GFP-CLASP2–9XS/A-positive signals inside clusters, which we observed in this work (or of GFP-CLIP-170-positive spots described earlier (13)), might actually represent contacts between the MT lattice and the cell cortex. These contacts could have been established at earlier time points when a growing MT end passed a particular spot in the cluster. It remains to be seen whether such MT lattice contacts also exist *in vivo*. Finally, because in the case of the GFP-CLASP2– 8XS/D mutant dots inside clusters lack any dynamic behavior, we propose that under normal conditions CLASP2-MT-membrane contacts inside clusters render proteins more dynamic, perhaps as a result of lateral movements of MTs.

Acknowledgments—We thank Dr. M. Ruegg, Basel, Switzerland, for critical reading of the manuscript, and Dr. O. Pertz and K. Martin (Basel) for their assistance with TIRF microscopy.

REFERENCES

1. McMahan, U. J., Horton, S. E., Werle, M. J., Honig, L. S., Kröger, S., Ruegg, M. A., and Escher, G. (1992) Agrin isoforms and their role in synaptogenesis. *Curr. Opin. Cell Biol.* **4,** 869–874
2. Sanes, J. R., and Lichtman, J. W. (1999) Development of the vertebrate neuromuscular junction. *Annu. Rev. Neurosci.* **22,** 389–442
3. Wu, H., Xiong, W. C., and Mei, L. (2010) To build a synapse: signaling pathways in neuromuscular junction assembly. *Development* **137,** 1017–1033
4. Kim, N., Stiegler, A. L., Cameron, T. O., Hallock, P. T., Gomez, A. M., Huang, J. H., Hubbard, S. R., Dustin, M. L., and Burden, S. J. (2008) Lrp4 is a receptor for agrin and forms a complex with MuSK. *Cell* **135,** 334–342
5. Zhang, B., Luo, S., Wang, Q., Suzuki, T., Xiong, W. C., and Mei, L. (2008) LRP4 serves as a coreceptor of agrin. *Neuron* **60,** 285–297
6. Cohen, I., Rimer, M., Lømo, T., and McMahan, U. J. (1997) Agrin-induced postsynaptic-like apparatus in skeletal muscle fibers *in vivo*. *Mol. Cell. Neurosci.* **9,** 237–253
7. Jones, G., Meier, T., Lichtsteiner, M., Witzemann, V., Sakmann, B., and Brenner, H. R. (1997) Induction by agrin of ectopic and functional postsynaptic-like membrane in innervated muscle. *Proc. Natl. Acad. Sci. U.S.A.* **94,** 2654–2659
8. Meier, T., Hauser, D. M., Chiquet, M., Landmann, L., Ruegg, M. A., and Brenner, H. R. (1997) Neural agrin induces ectopic postsynaptic specializations in innervated muscle fibers. *J. Neurosci.* **17,** 6534–6544
9. Chen, Y., Ip, F. C., Shi, L., Zhang, Z., Tang, H., Ng, Y. P., Ye, W. C., Fu, A. K., and Ip, N. Y. (2014) Coronin 6 regulates acetylcholine receptor clustering through modulating receptor anchorage to actin cytoskeleton. *J. Neurosci.* **34,** 2413–2421
10. Dai, Z., Luo, X., Xie, H., and Peng, H. B. (2000) The actin-driven movement and formation of acetylcholine receptor clusters. *J. Cell Biol.* **150,** 1321–1334
11. Geng, L., Qian, Y. K., Madhavan, R., and Peng, H. B. (2008) Transmembrane mechanisms in the assembly of the postsynaptic apparatus at the neuromuscular junction. *Chem. Biol. Interact.* **175,** 108–112
12. Hall, Z. W., Lubit, B. W., and Schwartz, J. H. (1981) Cytoplasmic actin in postsynaptic structures at the neuromuscular junction. *J. Cell Biol.* **90,** 789–792
13. Schmidt, N., Basu, S., Sladecek, S., Gatti, S., van Haren, J., Treves, S., Pielage, J., Galjart, N., and Brenner, H. R. (2012) Agrin regulates CLASP2-mediated capture of microtubules at the neuromuscular junction synaptic membrane. *J. Cell Biol.* **198,** 421–437
14. Akhmanova, A., Hoogenraad, C. C., Drabek, K., Stepanova, T., Dortland, B., Verkerk, T., Vermeulen, W., Burgering, B. M., De Zeeuw, C. I., Grosveld, F., and Galjart, N. (2001) CLASPs are CLIP-115 and -170 associating proteins involved in the regional regulation of microtubule dynamics in motile fibroblasts. *Cell* **104,** 923–935
15. Wittmann, T., and Waterman-Storer, C. M. (2005) Spatial regulation of CLASP affinity for microtubules by Rac1 and GSK3β in migrating epithelial cells. *J. Cell Biol.* **169,** 929–939
16. Watanabe, T., Noritake, J., Kakeno, M., Matsui, T., Harada, T., Wang, S., Itoh, N., Sato, K., Matsuzawa, K., Iwamatsu, A., Galjart, N., and Kaibuchi, K. (2009) Phosphorylation of CLASP2 by GSK-3β regulates its interaction with IQGAP1, EB1 and microtubules. *J. Cell Sci.* **122,** 2969–2979
17. Mimori-Kiyosue, Y., Grigoriev, I., Lansbergen, G., Sasaki, H., Matsui, C., Severin, F., Galjart, N., Grosveld, F., Vorobjev, I., Tsukita, S., and Akhmanova, A. (2005) CLASP1 and CLASP2 bind to EB1 and regulate microtubule plus-end dynamics at the cell cortex. *J. Cell Biol.* **168,** 141–153
18. Kumar, P., Chimenti, M. S., Pemble, H., Schönichen, A., Thompson, O., Jacobson, M. P., and Wittmann, T. (2012) Multisite phosphorylation disrupts arginine-glutamate salt bridge networks required for binding of cytoplasmic linker-associated protein 2 (CLASP2) to end-binding protein 1 (EB1). *J. Biol. Chem.* **287,** 17050–17064
19. Patel, K., Nogales, E., and Heald, R. (2012) Multiple domains of human CLASP contribute to microtubule dynamics and organization *in vitro* and in *Xenopus* egg extracts. *Cytoskeleton* **69,** 155–165
20. Kumar, P., Lyle, K. S., Gierke, S., Matov, A., Danuser, G., and Wittmann, T. (2009) GSK3β phosphorylation modulates CLASP-microtubule association and lamella microtubule attachment. *J. Cell Biol.* **184,** 895–908
21. Efimov, A., Kharitonov, A., Efimova, N., Loncarek, J., Miller, P. M., Andreyeva, N., Gleeson, P., Galjart, N., Maia, A. R., McLeod, I. X., Yates, J. R., 3rd, Maiato, H., Khodjakov, A., Akhmanova, A., and Kaverina, I. (2007) Asymmetric CLASP-dependent nucleation of noncentrosomal microtubules at the trans-Golgi network. *Dev. Cell* **12,** 917–930
22. Lansbergen, G., Grigoriev, I., Mimori-Kiyosue, Y., Ohtsuka, T., Higa, S., Kitajima, I., Demmers, J., Galjart, N., Houtsmuller, A. B., Grosveld, F., and Akhmanova, A. (2006) CLASPs attach microtubule plus ends to the cell cortex through a complex with LL5β. *Dev. Cell* **11,** 21–32
23. Kishi, M., Kummer, T. T., Eglen, S. J., and Sanes, J. R. (2005) LL5β. *J. Cell Biol.* **169,** 355–366
24. Blanco-Bose, W. E., Yao, C. C., Kramer, R. H., and Blau, H. M. (2001)

Purification of mouse primary myoblasts based on α7 integrin expression. *Exp. Cell Res.* **265,** 212–220
25. Schmidt, N., Akaaboune, M., Gajendran, N., Martinez-Pena y Valenzuela, I., Wakefield, S., Thurnheer, R., and Brenner, H. R. (2011) Neuregulin/ErbB regulate neuromuscular junction development by phosphorylation of α-dystrobrevin. *J. Cell Biol.* **195,** 1171–1184
26. Jones, G., Herczeg, A., Ruegg, M. A., Lichtsteiner, M., Kröger, S., and Brenner, H. R. (1996) Substrate-bound agrin induces expression of acetylcholine receptor ϵ-subunit gene in cultured mammalian muscle cells. *Proc. Natl. Acad. Sci. U.S.A.* **93,** 5985–5990
27. Lin, S., Landmann, L., Ruegg, M. A., and Brenner, H. R. (2008) The role of nerve *versus* muscle-derived factors in mammalian neuromuscular junction formation. *J. Neurosci.* **28,** 3333–3340
28. Schindelin, J., Arganda-Carreras, I., Frise, E., Kaynig, V., Longair, M., Pietzsch, T., Preibisch, S., Rueden, C., Saalfeld, S., Schmid, B., Tinevez, J. Y., White, D. J., Hartenstein, V., Eliceiri, K., Tomancak, P., and Cardona, A. (2012) Fiji: an open-source platform for biological-image analysis. *Nat. Methods* **9,** 676–682
29. Sugiyama, J. E., Glass, D. J., Yancopoulos, G. D., and Hall, Z. W. (1997) Laminin-induced acetylcholine receptor clustering: an alternative pathway. *J. Cell Biol.* **139,** 181–191
30. Drabek, K., van Ham, M., Stepanova, T., Draegestein, K., van Horssen, R., Sayas, C. L., Akhmanova, A., Ten Hagen, T., Smits, R., Fodde, R., Grosveld, F., and Galjart, N. (2006) Role of CLASP2 in microtubule stabilization and the regulation of persistent motility. *Curr. Biol.* **16,** 2259–2264
31. Al-Bassam, J., and Chang, F. (2011) Regulation of microtubule dynamics by TOG-domain proteins XMAP215/Dis1 and CLASP. *Trends Cell Biol.* **21,** 604–614
32. Maurer, S. P., Cade, N. I., Bohner, G., Gustafsson, N., Boutant, E., and Surrey, T. (2014) EB1 accelerates two conformational transitions important for microtubule maturation and dynamics. *Curr. Biol.* **24,** 372–384
33. Slep, K. C., and Vale, R. D. (2007) Structural basis of microtubule plus end tracking by XMAP215, CLIP-170, and EB1. *Mol. Cell* **27,** 976–991